Abstracta

Ano XVII - N. 04

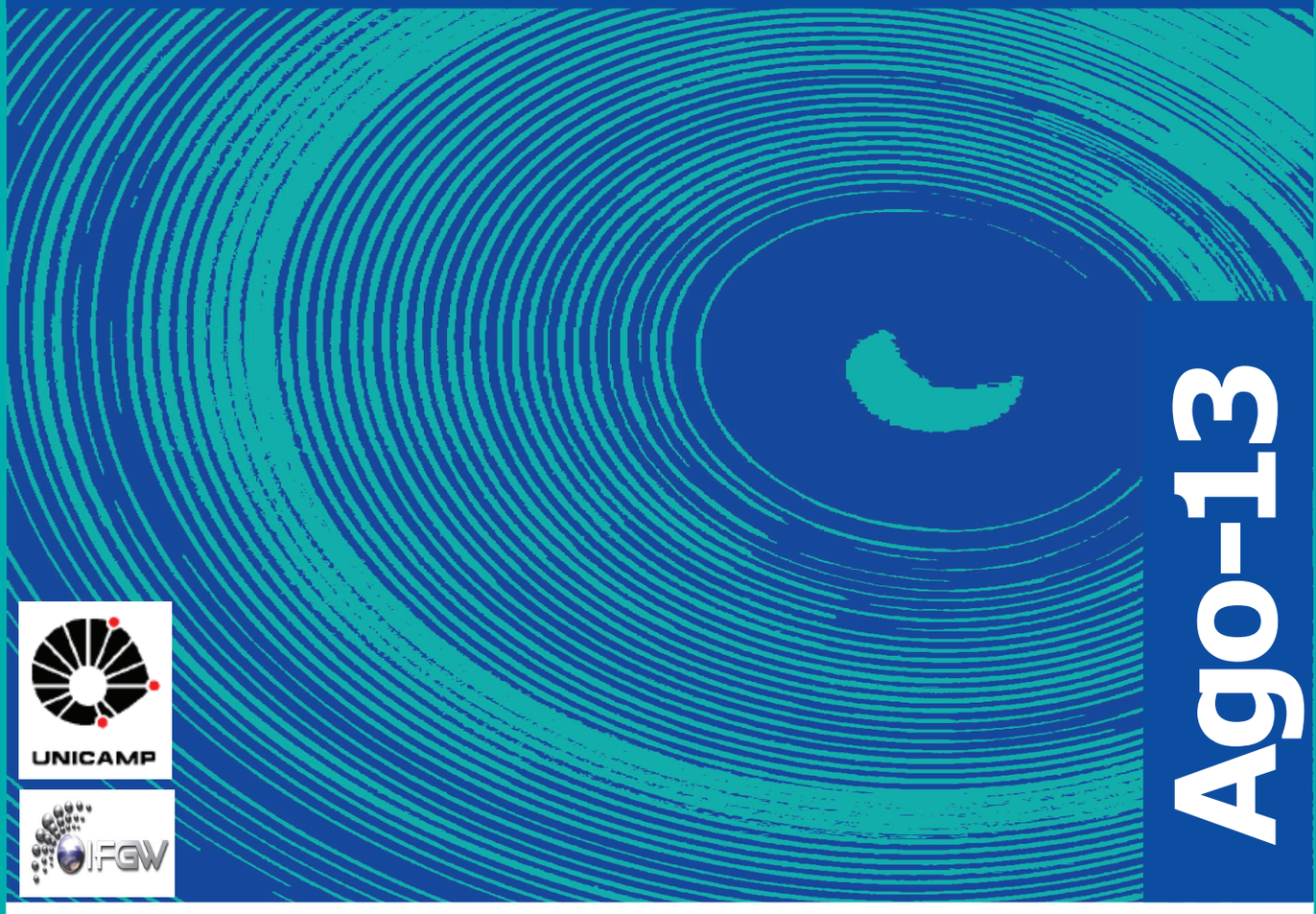

Ago-13

Trabalhos Publicados

[P189-2013] "A comparison between neutron-fluence measurements using metal-activation monitors and standard glasses calibrated via thin uranium-fission monitors and via eta q method"

Curvo, E. A. C.; Jonckheere, R.; **Guedes, S.*; Iunes, P. J.***; Tello, C. A.; **Hadler, J. C.***; Unterricker, S.; Ratschbacher, L.

The two fundamental approaches to fission-track dating involve either an explicit determination of the thermal neutron fluence (phi-method) or a calibration against age standards (zeta-method). The neutron fluence measurements are carried out with metal-activation monitors or with uranium-fission monitors, co-irradiated with the samples. Uranium-fission monitors consist of either a thin "mono-atomic") film, or a thick fission source (standard uranium glass) irradiated against a muscovite external track detector. In this work, different techniques for performing neutron-fluence measurements were compared: based on thin-film calibration, based on thick-source calibration, and based on gamma spectrometry of co-irradiated metal monitors (Au, Co). The results suggest that more experiments are needed to make all calibrations consistent, including new measurements of the length of etched induced tracks in mica. Also the standard glass calibration carried out with thin films should be confirmed with a greater number of calibrating irradiations.

Radiation Measurements 53-54, 38-44, 2013. DOI: 10.1016/j.radmeas.2013.03.002

[P190-2013] "Analysis of electrolytic hydrogen production models and distribution modes for public urban transport: study case in Foz do Iguacu, Brazil"

Riveros-Godoy, G. A.; Cavaliero, C.; **Silva, E.***

Currently, governments and companies aim their concern about the environmental problems and energy security. Within this context, the use of renewable hydrogen is presented as an interesting option. This paper presents the alternative to use a renewable resource abundant in the country: hydroelectricity. The public transport service in the urban area of Foz do Iguacu city, Brazil, was chosen as the scenario where a simulated replacement of the current diesel bus fleet with fuel cell buses was performed. The focus was to take advantage of the energy called Spilled Turbinable Energy (STE) verified by the ITAIPU Hydroelectric Power Plant from 2001 to 2006 in order to produce hydrogen by water electrolysis process. The paper does not contain thermodynamic analysis of the processes involved in the proposal. Based on the monthly average, the maximum value was 1,054,899 MWh and the minimum 9559 MWh. Evaluating the historic behavior of this potential energy in the considered period, from October to June, it was found that the energy demand to produce the electrolytic hydrogen needed to meet the whole demand of the public transport sector of Foz do Iguacu city, estimated in 14,454.3 MWh/month, amounts only between 1.5% to 8.5% of total spilled energy. This study presents two electrolytic hydrogen production models: the centralized and the decentralized associated with various distribution modes. The comparison between models shows that the centralized hydrogen production associated with central supply mode are economically more convenient for the city, and the hydrogen cost achieved was US$ 2.38/kg in contrast with the decentralized model associated with cryogenic liquid delivery which showed the highest cost, equal to US$ 4.61/kg. Finally, a sensitivity analysis was performed varying four parameters: equipment cost; rate of return; capital recovery time and electricity cost.

International Journal Of Energy Research 37[10], SI, 1142-1150, 2013. DOI: 10.1002/er.2972

[P191-2013] "Angular dependence of the photothermally modulated magnetic resonance in Gd thin films"

Soffner, M. E.; Guimares, A. O.; da Silva, E. C.; **Mansanares, A. M.***

In this paper we use electron spin resonance and photothermally modulated magnetic resonance techniques to investigate gadolinium thin films as a function of the orientation of the film surface with respect to the external magnetic field and of the temperature, around the magnetic phase transition temperature. We observe that, in the ferromagnetic phase, the resonance line is shifted up to higher external magnetic fields when the angle between the film surface and the field increases, revealing the magnetic anisotropy of the sample. At the same time, when the temperature is augmented to values higher than the phase transition temperature, the external field of the resonance collapses back to the expected value in the paramagnetic phase for all orientations. We also demonstrated that, even for the perpendicular orientation (magnetic field perpendicular to the sample surface), the photothermally modulated magnetic resonance signal is maximized near the magnetic phase transition temperature. Furthermore, in the ferromagnetic phase the photothermally modulated magnetic resonance intensity is very sensitive to the orientation, showing a significant enhancement in the perpendicular direction.

Applied Physics A-Materials Science & Processing 112[2], 403-409, 2013. DOI: 10.1007/s00339-012-7414-4

[P192-2013] "Argon Implantation in Tetrahedral Amorphous Carbon Deposited by Filtered Cathodic Vacuum Arc"

Marques, F. C.*; Viana, G. A.*; Motta, E. F.*; Silva, D. S.*; Wisnivesky, D.*; Cortes, A. D. S.*; Aguiar, M. R.*

The implantation of argon in tetrahedral amorphous carbon (ta-C), deposited by the filtered cathodic vacuum arc technique and concurrently bombarded with argon ions (Ar+), is investigated in this study. The ta-C films were prepared with a 5-ms DC-pulsed arc, a current of 190 A, and a frequency of 3 Hz, and they were deposited on a ground substrate holder. The argon atoms were implanted into the film by simultaneously bombarding the films with a beam of Ar+ in the 0-180 eV energy range. The concentration of argon, determined by Rutherford backscattering spectroscopy, was investigated as a function of the Ar+ energy. Raman scattering spectroscopy was used to investigate the structure of the films. The stress of the films depends on the Ar+ energy and reduces significantly as a function of the annealing temperature. A study of argon effusion, ranging from room temperature up to 1000 A degrees C, shows that the argon atoms evolve from the films at different temperatures depending on the Ar+ energy. Scanning electron microscopy revealed the formation of bubbles after argon effusion. It was observed that the structural transformations that promote the relaxation of the carbon matrix and the argon effusion are different from each other.

Journal Of Materials Engineering And Performance 22[5], 1396-1404, 2013. DOI: 10.1007/s11665-012-0401-2

[P193-2013] "Blood flow and oxygenation changes due to low-frequency repetitive transcranial magnetic stimulation of the cerebral cortex"

Mesquita, R. C.*; Faseyitan, O. K.; Turkeltaub, P. E.; Buckley, E. M.; Thomas, A.; Kim, M. N.; Durduran, T.; Greenberg, J. H.; Detre, J. A.; Yodh, A. G.; Hamilton, R. H.

Transcranial magnetic stimulation (TMS) modulates processing in the human brain and is therefore of interest as a treatment modality for neurologic conditions. During TMS administration, an electric current passing through a coil on the scalp creates a rapidly varying magnetic field that induces currents in the cerebral cortex. The effects of low-frequency (1 Hz), repetitive TMS (rTMS) on motor cortex cerebral blood flow (CBF) and tissue oxygenation in seven healthy adults,

during/after 20 min stimulation, is reported. Noninvasive optical methods are employed: diffuse correlation spectroscopy (DCS) for blood flow and diffuse optical spectroscopy (DOS) for hemoglobin concentrations. A significant increase in median CBF (33%) on the side ipsilateral to stimulation was observed during rTMS and persisted after discontinuation. The measured hemodynamic parameter variations enabled computation of relative changes in cerebral metabolic rate of oxygen consumption during rTMS, which increased significantly (28%) in the stimulated hemisphere. By contrast, hemodynamic changes from baseline were not observed contralateral to rTMS administration (all parameters, $p > 0.29$). In total, these findings provide new information about hemodynamic/metabolic responses to low-frequency rTMS and, importantly, demonstrate the feasibility of DCS/DOS for noninvasive monitoring of TMS-induced physiologic effects.

Journal Of Biomedical Optics 18[6], 067006, 2013. DOI: 10.1117/1.JBO.18.6.067006

[P194-2013] "Charge correlations using the balance function in Pb-Pb collisions at root s(NN)=2.76 TeV"

Abelev, B.; Adam, J.; Adamova, D.; Adare, A. M.; Aggarwal, M. M.; **Dash, A.*; Takahashi, J.***; et al.
ALICE Collaboration

In high-energy heavy-ion collisions, the correlations between the emitted particles can be used as a probe to gain insight into the charge creation mechanisms. In this Letter, we report the first results of such studies using the electric charge balance function in the relative pseudorapidity (Delta eta) and azimuthal angle (Delta phi) in Pb-Pb collisions at root s(NN) = 2.76 TeV with the ALICE detector at the Large Hadron Collider. The width of the balance function decreases with growing centrality (i.e. for more central collisions) in both projections. This centrality dependence is not reproduced by HIJING, while AMPT, a model which incorporates strings and parton rescattering, exhibits qualitative agreement with the measured correlations in Delta phi but fails to describe the correlations in Delta eta. A thermal blast-wave model incorporating local charge conservation and tuned to describe the p(T) spectra and v(2) measurements reported by ALICE, is used to fit the centrality dependence of the width of the balance function and to extract the average separation of balancing charges at freeze-out. The comparison of our results with measurements at lower energies reveals an ordering with root s(NN): the balance functions become narrower with increasing energy for all centralities. This is consistent with the effect of larger radial flow at the LHC energies but also with the late stage creation scenario of balancing charges. However, the relative decrease of the balance function widths in Delta eta and Delta phi, with centrality from the highest SPS to the LHC energy exhibits only small differences. This observation cannot be interpreted solely within the framework where the majority of the charge is produced at a later stage in the evolution of the heavy-ion collision.

Physics Letters B 723[4-5], 267-279, 2013. DOI: 10.1016/j.physletb.2013.05.039

[P195-2013] "D-Microfibers"

Beltran-Mejia, F.*; Osorio, J. H.*; Biazoli, C. R.*; Cordeiro, C. M. B.*

A simple mechanical setup was used to polish a standard single mode optical fiber in order to make it asymmetric. The polished fiber was tapered down maintaining the D-shape transversal profile. Its broken symmetry along with the extended evanescent field, due to the dimensions of the microfiber, implies a potentially high birefringent waveguide as well as a high-sensitivity external refractive index device. An experimental maximum sensitivity of S approximate to (3.0 +/- 0.2) x 10(4) nm/RIU was achieved, other experimental and numerical results supporting our initial assumptions are also presented.

Journal Of Lightwave Technology 31[16], 3056-3061, 2013. DOI: 10.1109/JLT.2013.2272915

[P196-2013] "Diffuse optical characterization of an exercising patient group with peripheral artery disease"

Mesquita, R. C.*; Putt, M.; Chandra, M.; Yu, G. Q.; Xing, X. M.; Han, S. W.; Lech, G.; Shang, Y.; Durduran, T.; Zhou, C.; Yodh, A. G.; Mohler, E. R.

Peripheral artery disease (PAD) is a common condition with high morbidity. While measurement of tissue oxygen saturation (StO2) has been demonstrated, this is the first study to assess both StO2 and relative blood flow (rBF) in the extremities of PAD patients. Diffuse optics is employed to measure hemodynamic response to treadmill and pedal exercises in 31 healthy controls and 26 patients. For StO2, mild and moderate/severe PAD groups show pronounced differences compared with controls. Pre-exercise mean StO2 is lower in PAD groups by 9.3% to 10.6% compared with means of 63.5% to 66.2% in controls. For pedal, relative rate of return of StO2 to baseline is more rapid in controls ($p < 0.05$). Patterns of rBF also differ among groups. After both exercises, rBF tend to occur at depressed levels among severe PAD patients compared with healthy ($p < 0.05$); post-treadmill, rBF tend to occur at elevated levels among healthy compared with severe PAD patients ($p < 0.05$). Additionally, relative rate of return to baseline StO2 is more rapid among subjects with reduced levels of depression in rBF ($p = 0.041$), even after adjustment for ankle brachial index. This suggests a physiologic connection between rBF and oxygenation that can be measured using diffuse optics, and potentially employed as an evaluative tool in further studies.

Journal Of Biomedical Optics 18[5], 057007, 2013. DOI: 10.1117/1.JBO.18.5.057007

[P197-2013] "Dissipation and theta(13) in neutrino oscillations"

Oliveira, R. L. N.*; Guzzo, M. M.*

We obtain a complete survival and transition probability involving three neutrino flavors when dissipation effects in vacuum are taken into consideration. In an approach that presents decoherence and relaxation effects, we study the behavior of the probabilities obtained from complete positivity constraints. Making the von Neumann entropy increase in time, many cases can be obtained and studied with the Lindblad master equation with addition of only one or two parameters related to dissipation. New possibilities are obtained when we take into account two decoherence parameters with different magnitudes which are given by reactor and accelerator neutrino oscillation experiments. We also present a model with only one parameter that has an important symmetry property, which can be used when the effective matter potential is important. Furthermore, the dissipation effects can contribute to the appearance of neutrinos that can hide or imitate the theta(13) effects and we study these possibilities showing that dissipative effects have an important role in three-neutrino oscillations.

European Physical Journal C 73[5], 2434, 2013. DOI: 10.1140/epjc/s10052-013-2434-6

[P198-2013] "Electroplated Bimagnetic Microwires: From Processing to Magnetic Properties and Sensor Devices"

Torrejon, J.; Infante, G.; Badini-Confalonieri, G.; **Pirota, K. R.***; Vazquez, M.

Multilayer microwires with biphase magnetic behavior are revisited in this work. They are fabricated by the combination of ultrarapid solidification and electroplating techniques, and they are composed by ferromagnetic nucleus, intermediate glass layer, and ferromagnetic outer shell.

Different magnetic configurations have been explored: soft/hard (CoFeSiB/CoNi and FeSiB/CoNi), soft/soft (CoFeSiB/FeNi), and hard/soft (FePtSi/FeNi). Their magnetic properties are mainly determined by the magnetic interactions between both magnetic phases: (I) a magnetoelastic coupling that arises from the mechanical stresses induced during the growth of the external magnetic shell and (II) a magnetostatic bias field that arises from uncompensated magnetic charges of the hard layer. Most outstanding static (i.e., low-field hysteresis loops) and dynamic (i.e., magnetoimpedance and ferromagnetic resonance) properties are reviewed in this article. The possibility to tailor the magnetization reversal of the soft phase through the tuning of those magnetic couplings places multilayer biphase microwires in a very competitive position as functional sensing elements suitable for a number of technological applications. In particular, we focus on their use in multifunctional sensor devices and fluxgate applications.

JOM 65[7], 890-900, 2013. DOI: 10.1007/s11837-013-0614-3

[P199-2013] "Elliptic flow of identified hadrons in Au + Au collisions at root s(NN)=7.7-62.4 GeV"

Adamczyk, L.; Adkins, J. K.; Agakishiev, G.; Aggarwal, M. M.; **Derradi de Souza, R.*; Takahashi, J.*; Vasconcelos, G. M. S.***, et al.
STAR Collaboration

Measurements of the elliptic flow, upsilon(2), of identified hadrons (pi(+/-), K-+/-, K-s(0), p, (p) over bar, phi, Lambda, (Lambda) over bar, Xi(-), (Xi) over bar (+), Omega(-), (Omega) over bar (+)) in Au + Au collisions at root s(NN) = 7.7, 11.5, 19.6, 27, 39, and 62.4 GeV are presented. The measurements were done at midrapidity using the time-projection chamber and the time-of-flight detectors of the Solenoidal Tracker at RHIC experiment during the beam-energy scan program at Relativistic Heavy Ion Collider. A significant difference in the upsilon(2) values for particles and the corresponding antiparticles was observed at all transverse momenta for the first time. The difference increases with decreasing center-of-mass energy, root s(NN) (or increasing baryon chemical potential, mu(B)), and is larger for the baryons as compared to the mesons. This implies that particles and antiparticles are no longer consistent with the universal number-of-constituent quark (NCQ) scaling of upsilon(2) that was observed at root s(NN) = 200 GeV. However, for the selected group of particles (p(+), K+, K-s(0), p, Lambda, Xi(-), Omega(-)) NCQ scaling at (m(T) - m(0))/n(q) > 0.4 GeV/c(2) is not violated within +/- 10%. The upsilon(2) values for f mesons at 7.7 and 11.5 GeV are approximately two standard deviations from the trend defined by the other hadrons at the highest measured p(T) values.

Physical Review C 88[1], 014902, 2013. DOI: 10.1103/PhysRevC.88.014902

[P200-2013] "Energy deposition in small-scale targets of liquid water using the very low energy electromagnetic physics processes of the Geant4 toolkit"

Incerti, S.; Champion, C.; Tran, H. N.; **Karamitros, M.*; Bernal, M.*;** Francis, Z.; Ivanchenko, V.; Mantero, A.
Geant4-DNA Collaboration

In the perspective of building an open source simulation platform dedicated to the modelling of early biological molecular damages due to ionising radiation at the DNA scale, the general-purpose Geant4 Monte Carlo simulation toolkit has been recently extended with specific very low energy electromagnetic physics processes for liquid water medium. These processes - also called "Geant4-DNA" processes - simulate the physical interactions induced by electrons, hydrogen and helium atoms of different charge states. The present work reports on the energy deposit distributions obtained for incident electrons, protons and alpha particles in nanometre-size volumes comparable to those present in the genetic material of mammalian cells. The frequency distributions of the energy deposition obtained for three typical geometries of nanometre-size cylindrical targets placed in a spherical phantom are found to be in reasonable agreement with prior works. Furthermore, we present a combination of the Geant4-DNA processes with a simplified geometrical model of a cellular nucleus allowing the evaluation of energy deposits in volumes of biological interest.

Nuclear Instruments & Methods In Physics Research Section B-Beam Interactions With Materials And Atoms 306, 158-164, 2013. DOI: 10.1016/j.nimb.2012.12.054

[P201-2013] "Exploring nu(tau) - nu(s) mixing with cascade events in DeepCore"

Esmaili, A.*; Halzen, F.; **Peres, O. L. G.***

The atmospheric neutrino data collected by the IceCube experiment and its low-energy extension DeepCore provide a unique opportunity to probe the neutrino sector of the Standard Model. In the low energy range the experiment have observed neutrino oscillations, and the high energy data are especially sensitive to signatures of new physics in the neutrino sector. In this context, we previously demonstrated the unmatched potential of the experiment to reveal the existence of light sterile neutrinos. The studies are routinely performed in the simplest 3 + 1 model concentrating on disappearance of muon neutrinos of TeV energy as a result of their mixing with a sterile neutrino. We here extend this analysis to include cascade events that are secondary electromagnetic and hadronic showers produced by neutrinos of all flavors. We find that it is possible to probe the complete parameter space of 3 + 1 model, including the poorly constrained mixing of the sterile neutrino to tau neutrinos. We show that nu(tau) - nu(s) mixing results into a unique signature in the data that will allow IceCube to obtain constraints well below the current upper limits.

Journal Of Cosmology And Astroparticle Physics 7[048], 2013. DOI: 10.1088/1475-7516/2013/07/048

[P202-2013] "Fast oxidative pyrolysis of sugar cane straw in a fluidized bed reactor"

Mesa-Perez, J. M.; Rocha, J. D.; Barbosa-Cortez, L. A.; Penedo-Medina, M.; **Luengo, C. A.***; Cascarosa, E.

This study focuses on the technical viability evaluation of the fast pyrolysis of sugar cane straw for its energy use. By means of this thermochemical process, the sugar cane straw is converted into bio-fuels (biochar, bio-oil) and non-condensable gases. The bio-fuels obtained could be used as fuel or as raw material in the chemical industry. The fast pyrolysis of sugar cane straw has been developed in a fluidized bed reactor. In order to improve this process to obtain high bio-oil yield, the influence of the operational conditions (equivalence ratio and temperature) on the product yields and on their characteristics was evaluated. The product yields of bio-oil and char were up to 35.5 wt.% and 48.2 wt.% respectively. The maximum bio-oil yield was achieved at temperature and equivalence ratio conditions of 470 degrees C and 0.14. The bio-oil obtained has low oxygen content (38.48 wt.% dry basis), very low water content, and a lower heating value of 22.95 MJ/kg. The gas chromatographic analyses allowed the identification of oxygenated compounds and heterocyclic aromatic hydrocarbons. The bio-oil pH ranged between 3.14 and 3.57 due to the presence of acid organic compounds. The char obtained has a high fixed carbon and volatile matter content. Its HHV value is 13.54 MJ/kg.

Applied Thermal Engineering 56[1-2], 167-175, 2013. DOI: 10.1016/j.applthermaleng.2013.03.017

[P203-2013] "Fine structure of a biexciton in a single quantum dot with a magnetic impurity"

Trojnar, A. H.; Korkusinski, M.; **Mendes, U. C.***; Goryca, M.; Koperski, M.; Smolenski, T.; Kossacki, P.; Wojnar, P.; Hawrylak, P.

We show theoretically and experimentally that the ground state of a biexciton in a CdTe self-assembled quantum dot with a magnetic Mn impurity exhibits a fine structure due to electron-electron Coulomb and electron-Mn exchange interactions. Results of exact diagonalization of the microscopic biexciton-manganese-ion model predict a pattern of three pairs of states in the ground-state manifold, each pair labeled by the projection of Mn spin. We show that the fine structure determines the ordering of the biexciton emission maxima and can be derived from the biexciton and exciton emission spectra. Theoretical predictions are successfully compared with measured biexciton and exciton emission spectra of a single CdTe dot with a Mn ion in its center.

Physical Review B 87[20], 205311, 2013. DOI: 10.1103/PhysRevB.87.205311

[P204-2013] "First measurement of theta(13) from delayed neutron capture on hydrogen in the Double Chooz experiment"

Abe, Y.; Aberleu, C.; dos Anjos, J. C.; Barriere, J. C.; Bergevin, M.; Bernstein, A.; **Gonzalez, L. F. G.*; Kemp, E.***; et al.

The Double Chooz experiment has determined the value of the neutrino oscillation parameter theta(13) from an analysis of inverse beta decay interactions with neutron capture on hydrogen. This analysis uses a three times larger fiducial volume than the standard Double Chooz assessment, which is restricted to a region doped with gadolinium (Gd), yielding an exposure of 113.1 GW-ton-years. The data sample used in this analysis is distinct from that of the Gd analysis, and the systematic uncertainties are also largely independent, with some exceptions, such as the reactor neutrino flux prediction. A combined rate- and energy-dependent fit finds sin(2) 2 theta(13) = 0.097 +/- 0.034 (stat.) +/- 0.034 (syst.), excluding the no-oscillation hypothesis at 2.0 sigma. This result is consistent with previous measurements of sin(2) 2 theta(13).

Physics Letters B 723[1-3], 66-70, 2013. DOI: 10.1016/j.physletb.2013.04.050

[P205-2013] "Ghost propagator and ghost-gluon vertex from Schwinger-Dyson equations"

Aguilar, A. C.*; Ibanez, D.; Papavassiliou, J.

We study an approximate version of the Schwinger-Dyson equation that controls the nonperturbative behavior of the ghost--gluon vertex in the Landau gauge. In particular, we focus on the form factor that enters in the dynamical equation for the ghost dressing function, in the same gauge, and derive its integral equation, in the "one-loop dressed" approximation. We consider two special kinematic configurations, which simplify the momentum dependence of the unknown quantity; in particular, we study the soft gluon case and the well-known Taylor limit. When coupled with the Schwinger-Dyson equation of the ghost dressing function, the contribution of this form factor provides considerable support to the relevant integral kernel. As a consequence, the solution of this coupled system of integral equations furnishes a ghost dressing function that reproduces the standard lattice results rather accurately, without the need to artificially increase the value of the gauge coupling.

Physical Review D 87[11], 114020, 2013. DOI: 10.1103/PhysRevD.87.114020

[P206-2013] "Implantation of xenon in amorphous carbon and silicon for brachytherapy application"

Marques, F. C.*; Barbieri, P. F.*; Viana, G. A.*; da Silva, D. S.*

We report a procedure to implant high dose of xenon atoms (Xe) in amorphous carbon, a-C, and amorphous silicon, a-Si, for application in brachytherapy seeds. An ion beam assisted deposition (IBAD) system was used for the deposition of the films, where one ion gun was used for sputtering a carbon (or silicon) target, while the other ion gun was used to simultaneously bombard the growing film with a beam of xenon ion Xe+ in the 0-300 eV range. Xe atoms were implanted into the film with concentration up to 5.5 at.%, obtained with Xe bombardment energy in the 50-150 eV range. X-ray absorption spectroscopy was used to investigate the local arrangement of the implanted Xe atoms through the Xe L-III absorption edge (4.75 keV). It was observed that Xe atoms tend to agglomerate in nanoclusters in a-C and are dispersed in a-Si.

Applied Surface Science 275[156-159], 2013. DOI: 10.1016/j.apsusc.2013.01.054

[P207-2013] "Influence of probe pressure on the diffuse correlation spectroscopy blood flow signal: extra-cerebral contributions"

Mesquita, R. C.*; Schenkel, S. S.; Minkoff, D. L.; Lu, X. P.; Favilla, C. G.; Vora, P. M.; Busch, D. R.; Chandra, M.; Greenberg, J. H.; Detre, J. A.; Yodh, A. G.

A pilot study explores relative contributions of extra-cerebral (scalp/skull) versus brain (cerebral) tissues to the blood flow index determined by diffuse correlation spectroscopy (DCS). Microvascular DCS flow measurements were made on the head during baseline and breath-holding/hyperventilation tasks, both with and without pressure. Baseline (resting) data enabled estimation of extra-cerebral flow signals and their pressure dependencies. A simple two-component model was used to derive baseline and activated cerebral blood flow (CBF) signals, and the DCS flow indices were also cross-correlated with concurrent Transcranial Doppler Ultrasound (TCD) blood velocity measurements. The study suggests new pressure--dependent experimental paradigms for elucidation of blood flow contributions from extra-cerebral and cerebral tissues.

Biomedical Optics Express 4[7], 978-994, 2013. DOI: 10.1364/BOE.4.000978

[P208-2013] "J/psi production at high transverse momenta in p plus p and Au plus Au collisions at root s(NN)=200 GeV"

Adamczyk, L.; Agakishiev, G.; Aggarwal, M. M.; Ahammed, Z.; **Derradi de Souza, R.*; Takahashi, J.*; Vasconcelos, G. M. S.***, et al.
STAR Collaboration

We report J/psi spectra for transverse momenta P-T > 5 GeV/c at mid-rapidity in p + p and Au + Au collisions at root s(NN) = 200 GeV. The inclusive J/psi spectrum and the extracted B-hadron feed-down are compared to models incorporating different production mechanisms. We observe significant suppression of the J/psi yields for p(T) > 5 GeV/c in 0-30% central Au + Au collisions relative to the p + p yield scaled by the number of binary nucleon-nucleon collisions in Au + Au collisions. In 30-60% mid--central collisions, no such suppression is observed. The level of suppression is consistently less than that of high-p(T) pi(+/-) and low-p(T) J/psi at RHIC and high-p(T) J/psi at the LHC.

Physics Letters B 722[1-3], 55-62, 2013. DOI: 10.1016/j.physletb.2013.04.010

[P209-2013] "Laser irradiation of carbon nanotube films: Effects and heat dissipation probed by Raman spectroscopy"

Mialichi, J. R.*; Brasil, M. J. S. P.*; Iikawa, F.*; Verissimo, C.; Moshkalev, S. A.

We investigate the thermal properties of thin films formed by single- and multi-walled carbon nanotubes submitted to laser irradiation using Raman scattering as a probe of both the tube morphology and the local temperature. The nanotubes were submitted to heating/cooling cycles attaining high laser intensities (similar to 1.4 MW/cm(2)) under vacuum and in the presence of an atmosphere, with and without oxygen. We investigate the heat diffusion of the irradiated nanotubes to their surroundings and the effect of laser annealing on their properties. The presence of oxygen during laser irradiation gives rise to an irreversible increase of the Raman efficiency of the carbon nanotubes and to a remarkable increase of the thermal conductivity of multi-walled films. The second effect can be applied to design thermal conductive channels in devices based on carbon nanotube films using laser beams.

Journal Of Applied Physics 114[2], 024904, 2013. DOI: 10.1063/1.4813485

[P210-2013] "Licensing a fuel cell bus and a hydrogen fueling station in Brazil"

Neves, N. P., Jr.*; Pinto, C. S.

The Brazilian Fuel Cell Bus Project is being developed by a consortium comprising 14 national and international partners. The project was initially supported by the GEF/UNDP and MME/FINEP Brazil. The national coordination is under responsibility of MME and EMTU/SP, the Sao Paulo Metropolitan Urban Transport Company that also controls the bus operation and bus routes. This work reports the efforts done in order to obtain the necessary licenses to operate the first fuel cell buses for regular service in Brazil, as well as the first commercial hydrogen fueling station to attend the vehicles.

International Journal Of Hydrogen Energy 38[19], 8215-8220, 2013. DOI: 10.1016/j.ijhydene.2013.01.035

[P211-2013] "Low-energy electron collisions with thiophene"

da Costa, R. F.; Varella, M. T. do N.; **Lima, M. A. P.***; Bettega, M. H. F.

We report on elastic integral, momentum transfer, and differential cross sections for collisions of low-energy electrons with thiophene molecules. The scattering calculations presented here used the Schwinger multichannel method and were carried out in the static-exchange and static-exchange plus polarization approximations for energies ranging from 0.5 eV to 6 eV. We found shape resonances related to the formation of two long-lived pi* anion states. These resonant structures are centered at the energies of 1.00 eV (2.85 eV) and 2.82 eV (5.00 eV) in the static-exchange plus polarization (static-exchange) approximation and belong to the B-1 and A(2) symmetries of the C-2v point group, respectively. Our results also suggest the existence of a sigma* shape resonance in the B-2 symmetry with a strong d-wave character, located at around 2.78 eV (5.50 eV) as obtained in the static-exchange plus polarization (static-exchange) calculation. It is worth to mention that the results obtained at the static-exchange plus polarization level of approximation for the two pi* resonances are in good agreement with the electron transmission spectroscopy results of 1.15 eV and 2.63 eV measured by Modelli and Burrow [J. Phys. Chem. A 108, 5721 (2004)]. The existence of the sigma* shape resonance is in agreement with the observations of Dezarnaud-Dandiney et al. [J. Phys. B 31, L497 (1998)] based on the electron transmission spectra of dimethyl(poly) sulphides. A comparison among the resonances of thiophene with those of pyrrole and furan is also performed and, altogether, the resonance spectra obtained for these molecules point out that electron attachment to pi* molecular orbitals is a general feature displayed by these five-membered heterocyclic compounds.

Journal Of Chemical Physics 138[19], 194306, 2013. DOI: 10.1063/1.4805107

[P212-2013] "Magnetic and Electric Orderings and Intrinsic Magnetoelectric Coupling in Pb(Fe,W)O-3 Based Ceramics"

Fraygola, B.; **Coelho, A. A.***; Eiras, J. A.

In this work structural, electric, dielectric, and anelastic properties of single phase high density (> 97%) (1-x) PFW--xPT ceramics, with 0 <= x <= 0.30, are investigated. The experimental results show that the temperatures, in which magnetic (T-N) or electric (T-FE) ordering occur, can be interchanged by PbTiO3 addition. Correlations between the experimental results allow to estimate intrinsic ferromagnetoelectroelastic coefficients at the temperatures, where the multiferroic state exist. The intrinsic magnetoelectric coefficient is maximum for compositions, in which the temperatures for magnetic and ferroelectric ordering coincide, no matter in what sequence the orderings (FE or AFM) occur.

Ferroelectrics 442[1], 50-60, 2013. DOI: 10.1080/00150193.2013.773877

[P213-2013] "Magnetic polaron effect in Sr8-xEuxGa16Ge30 clathrates probed by electron spin resonance"

Rosa, P. F. S.*; Iwamoto, W.*; Holanda, L. M.*; Ribeiro, R. A.; **Pagliuso, P. G.*; Rettori, C.***; Avila, M. A.

Single crystals of the type-I clathrate series Sr8-xEuxGa16Ge30 (x = 0.01-8) were grown by Ga flux and systematically studied by magnetic susceptibility, electrical resistivity, and electron spin resonance (ESR) measurements. Both magnetic transition temperatures (T-c and T*) were mapped as a function of x. We found that the Curie temperature (T-c) and the magnetic anomaly temperature (T*) decrease systematically as Eu is substituted by Sr until no ordering is observed above 2 K for x = 1.0. For samples where the rattling Einstein temperature of theta(E) approximate to 25-60 K lies above T-c, we have observed no features in the ESR data, suggesting that the Eu2+ 4f spin dynamics is weakly coupled to the rattling modes. As the temperature is lowered and the magnetic field is increased, the ESR linewidth (Delta H) behavior points to the formation of magnetic polarons.

Physical Review B 87[22], UNSP 224414, 2013. DOI: 10.1103/PhysRevB.87.224414

[P214-2013] "Magnetic properties study of iron-oxide nanoparticles/PVA ferrogels with potential biomedical applications"

Zelis, P. M.; **Muraca, D.*;** Gonzalez, J. S.; Pasquevich, G. A.; Alvarez, V. A.; **Pirota, K. R.***; Sanchez, F. H.

A study of the magnetic behavior of maghemite nanoparticles (NPs) in polyvinyl alcohol (PVA) polymer matrices prepared by physical cross-linking is reported. The magnetic nanocomposites (ferrogels) were obtained by the in situ co-precipitation of iron salts in the presence of PVA polymer, and subsequently subjected to freezing-thawing cycles. The magnetic behavior of these ferrogels was compared with that of similar systems synthesized using the glutaraldehyde. This type of chemical cross-linking agents presents several disadvantages due to the presence of residual toxic molecules in the gel, which are undesirable for biological applications. Characteristic particle size determined by several techniques are in the range 7.9-9.3 nm.

The iron oxidation state in the NPs was studied by X-ray absorption spectroscopy. Mossbauer measurements showed that the NP magnetic moments present collective magnetic excitations and superparamagnetic relaxations. The blocking and irreversibility temperatures of the NPs in the ferrogels, and the magnetic anisotropy constant, were obtained from magnetic measurements. An empirical model including two magnetic contributions (large NPs slightly departed from thermodynamic equilibrium below 200 K, and small NPs at thermodynamic equilibrium) was used to fit the experimental magnetization curves. A deviation from the superparamagnetic regime was observed. This deviation was explained on the basis of an interacting superparamagnetic model. From this model, relevant magnetic and structural properties were obtained, such as the magnitude order of the dipolar interaction energy, the NPs magnetic moment, and the number of NPs per ferrogel mass unit. This study contributes to the understanding of the basic physics of a new class of materials that could emerge from the PVA-based magnetic ferrogels.

Journal Of Nanoparticle Research 15[5], 1613, 2013. DOI: 10.1007/s11051-013-1613-6

[P215-2013] "Measurement of inelastic, single- and double--diffraction cross sections in proton-proton collisions at the LHC with ALICE"

Abelev, B.; Adam, J.; Adamova, D.; Adare, A. M.; **Chinellato, D. D.*; Dash, A.*; Takahashi, J.*;** et al.
ALICE Collaboration

Measurements of cross sections of inelastic and diffractive processes in proton-proton collisions at LHC energies were carried out with the ALICE detector. The fractions of diffractive processes in inelastic collisions were determined from a study of gaps in charged particle pseudorapidity distributions: for single diffraction (diffractive mass M-X < 200 GeV/c(2)) sigma(SD)/sigma(INEL) = 0.21 +/- 0.03, 0.20(-0.08)(+0.07,) and 0.20(-0.07)(+0.04), respectively at centre-of-mass energies root s = 0.9, 2.76, and 7 TeV; for double diffraction (for a pseudorapidity gap Delta eta > 3) sigma(DD)/sigma(INEL) = 0.11 +/- 0.03, 0.12 +/- 0.05, and 0.12(-0.04)(+0.05), respectively at root s = 0.9, 2.76, and 7 TeV. To measure the inelastic cross section, beam properties were determined with van der Meer scans, and, using a simulation of diffraction adjusted to data, the following values were obtained: sigma(INEL) = 62.8(-4.0)(+2.4)(model) +/- 1.2(lumi) mb at root s = 2.76 TeV and 73.2(-4.6)(+2.0)(model) +/- 2.6(lumi) mb at root s = 7 TeV. The single- and double-diffractive cross sections were calculated combining relative rates of diffraction with inelastic cross sections. The results are compared to previous measurements at proton-antiproton and proton-proton colliders at lower energies, to measurements by other experiments at the LHC, and to theoretical models.

European Physical Journal C 73[6], 2456, 2013. DOI: 10.1140/epjc/s10052-013-2456-0

[P216-2013] "Measurement of Neutrino and Antineutrino Oscillations Using Beam and Atmospheric Data in MINOS"

Adamson, P.; Anghel, I.; Backhouse, C.; Barr, G.; **Coelho, J. A. B.*; Escobar, C. O.***; et al.
MINOS Collaboration

We report measurements of oscillation parameters from v(mu) and (v) over bar (mu) disappearance using beam and atmospheric data from MINOS. The data comprise exposures of 10.71 X 10(20) protons on target in the v(mu)-dominated beam, 3.36 X 10(20) protons on target in the (v) over bar (mu)--enhanced beam, and 37.88 kton yr of atmospheric neutrinos. Assuming identical v and (v) over bar oscillation parameters, we measure vertical bar Delta m(2)vertical bar = (2.41(-0.10)(+0.09)) X 10(-3) eV(2) and sin(2)(2 theta) = 0.950(-0.036)(+0.035). Allowing independent v and (v) over bar oscillations, we measure antineutrino parameters of vertical bar(m) over bar (2)vertical bar = (2.50(-0.250)(+0.23)) X 10(-3) eV(2) and sin(2)(2 (theta) over bar) = 0.97(-0.08)(+0.03), with minimal change to the neutrino parameters.

Physical Review Letters 110[25], 251801, 2013. DOI: 10.1103/PhysRevLett.110.251801

[P217-2013] "Measurement of the inclusive differential jet cross section in pp collisions at root s=2.76 TeV"

Abelev, B.; Adam, J.; Adamova, D.; Adare, A. M.; Aggarwal, M. M.; **Dash, A.*; Takahashi, I. J.*;** et al.
ALICE Collaboration

The ALICE Collaboration at the CERN Large Hadron Collider reports the first measurement of the inclusive differential jet cross section at mid-rapidity in pp collisions at root s = 2.76 TeV, with integrated luminosity of 13.6 nb(-1). Jets are measured over the transverse momentum range 20 to 125 GeV/c and are corrected to the particle level. Calculations based on Next-to-Leading Order perturbative QCD are in good agreement with the measurements. The ratio of inclusive jet cross sections for jet radii R = 0.2 and R = 0.4 is reported, and is also well reproduced by a Next-to-Leading Order perturbative QCD calculation when hadronization effects are included.

Physics Letters B 722[4-5], 262-272, 2013. DOI: 10.1016/j.physletb.2013.04.026

[P218-2013] "Mesoscopic hydro-thermodynamics of phonons"

Vasconcellos, A. R.*; de Castro, A. R. B.*; Silva, C. A. B.; **Luzzi, R.***

A generalized Hydrodynamics, referred to as Mesoscopic Hydro-Thermodynamics, of phonons in semiconductors is presented. It involves the descriptions of the motion of the quasi-particle density and of the energy density. The hydrodynamic equations, which couple both types of movement via thermo-elastic processes, are derived starting with a generalized Peierls-Boltzmann kinetic equation obtained in the framework of a Non-Equilibrium Statistical Ensemble Formalism, providing such Mesoscopic Hydro-Thermodynamics. The case of a contraction in first order is worked out in detail. The associated Maxwell times are derived and discussed. The densities of quasi-particles and of energy are found to satisfy coupled Maxwell-Cattaneo-like (hyperbolic) equations. The analysis of thermo-elastic effects is done and applied to investigate thermal distortion in silicon mirrors under incidence of high intensity X-ray pulses in FEL facilities. The derivation of a generalized Guyer-Krumhansl equation governing the flux of heat and the associated thermal conductivity coefficient is also presented.

Aip Advances 3[7], 072106, 2013. DOI: 10.1063/1.4813835

[P219-2013] "Microstructure and Thermal Profile of Structured Lipids Produced by Continuous Enzymatic Interesterification"

da Silva, R. C.; Ribeiro, A. P. B.; Soares, F. A. S. M.; Capacla, I. R.; Hazzan, M.; dos Santos, A. O.; **Cardoso, L. P.***; Gioielli, L. A.

Enzymatic interesterification has been shown to be an alternative for the production of structured lipids resembling human milk fat. The knowledge of the physical properties of fat is an important tool for the implementation of this fat in a food matrix. The enzymatic interesterification reaction modifies the composition of triacylglycerols changing the crystallization properties and polymorphic form of fats. Blends containing different proportions of lard and soybean oil (80:20, 70:30, 40:60, 30:70 and 20:80)

were enzymatically interesterified in a continuous flow tubular reactor and analyzed for crystalline structure by polarized light microscopy, the polymorphic form using X-ray diffraction and thermal properties by differential scanning calorimetry. The structural modifications resulting from continuous enzymatic interesterification changed the crystallization behavior and thermal profile of the samples, reducing enthalpy values. Structural changes were also evident on polarized light microscopy images, disclosing an increase in the crystallization rate among the samples after the continuous enzymatic reaction.

Journal Of The American Oil Chemists Society 90[5], 631-639, 2013. DOI: 10.1007/s11746-013-2208-1

[P220-2013] "Multiplicity and transverse momentum dependence of two- and four-particle correlations in pPb and PbPb collisions"

Chatrchyan, S.; Khachatryan, V.; Sirunyan, A. M.; Tumasyan, A.; **Chinellato, J.*; Tonelli Manganote, E. J.*;** et al.
CMS Collaboration

Measurements of two- and four-particle angular correlations for charged particles emitted in pPb collisions are presented over a wide range in pseudorapidity and full azimuth. The data, corresponding to an integrated luminosity of approximately 31 nb(-1), were collected during the 2013 LHC pPb run at a nucleon-nucleon center-of-mass energy of 5.02 TeV by the CMS experiment. The results are compared to 2.76 TeV semi-peripheral PbPb collision data, collected during the 2011 PbPb run, covering a similar range of particle multiplicities. The observed correlations are characterized by the near-side (vertical bar Delta phi vertical bar approximate to 0) associated pair yields and the azimuthal anisotropy Fourier harmonics (nu(n)). The second-order (nu(2)) and third-order (v(3)) anisotropy harmonics are extracted using the two-particle azimuthal correlation technique. A four-particle correlation method is also applied to obtain the value of nu(2) and further explore the multi-particle nature of the correlations. Both associated pair yields and anisotropy harmonics are studied as a function of particle multiplicity and transverse momentum. The associated pair yields, the four-particle nu(2), and the nu(3) become apparent at about the same multiplicity. A remarkable similarity in the nu(3) signal as a function of multiplicity is observed between the pPb and PbPb systems. Predictions based on the color glass condensate and hydrodynamic models are compared to the experimental results.

Physics Letters B 724[4-5], 213-240, 2013. DOI: 10.1016/j.physletb.2013.06.028

[P221-2013] "Observation of a new boson with mass near 125 GeV in pp collisions at root s=7 and 8 TeV"

Chatrchyan, S.; Khachatryan, V.; Sirunyan, A. M.; Tumasyan, A.; **Chinellato, J.*; Tonelli Manganote, E. J.***; et al.
CMS Collaboration

A detailed description is reported of the analysis used by the CMS Collaboration in the search for the standard model Higgs boson in pp collisions at the LHC, which led to the observation of a new boson. The data sample corresponds to integrated luminosities up to 5.1 fb(-1) at root s = 7 TeV, and up to 5.3 fb(-1) at root s = 8 TeV. The results for five Higgs boson decay modes gamma gamma, ZZ, WW, tau tau, and bb, which show a combined local significance of 5 standard deviations near 125 GeV, are reviewed. A fit to the invariant mass of the two high resolution channels, gamma gamma and ZZ -> 4l, gives a mass estimate of 125.3 +/- 0.4 (stat.) +/- 0.5 (syst.) GeV. The measurements are interpreted in the context of the standard model Lagrangian for the scalar Higgs field interacting with fermions and vector bosons. The measured values of the corresponding couplings are compared to the standard model predictions. The hypothesis of custodial symmetry is tested through the measurement of the ratio of the couplings to the W and Z bosons. All the results are consistent, within their uncertainties, with the expectations for a standard model Higgs boson.

Journal Of High Energy Physics 6, 081, 2013. DOI: 10.1007/JHEP06(2013)081

[P222-2013] "On the rise of proton-proton cross-sections at high energies"

Fagundes, D. A.*; Menon, M. J.*; Silva, P. V. R. G.*

The rise of total, elastic and inelastic hadronic cross sections at high energies is investigated by means of an analytical parametrization, with the exponent of the leading logarithm contribution as a free fit parameter. Using derivative dispersion relations with one subtraction, two different fits to proton-proton and antiproton-proton total cross section and. parameter data are developed, reproducing well the experimental information in the energy region 5 GeV-7 TeV. The parametrization for the total cross sections is then extended to fit the elastic (integrated) cross section data in the same energy region, with satisfactory results. From these empirical results we extract the energy dependence of several physical quantities: inelastic cross section, ratios elastic/total, inelastic/total cross sections, ratio total-cross-section/elastic-slope, elastic slope and optical point. All data, fitted and predicted, are quite well described. We find a statistically consistent solution indicating: (1) an increase of the hadronic cross sections with the energy faster than the log-squared bound by Froissart and Martin; (2) asymptotic limits 1/3 and 2/3 for the ratios elastic/total and inelastic/total cross sections, respectively; a result in agreement with unitarity. These indications corroborate recent theoretical arguments by Azimov on the rise of the total cross section.

Journal Of Physics G-Nuclear and Particle Physics 40[6], 065005, 2013. DOI: 10.1088/0954-3899/40/6/065005

[P223-2013] "Optical sensor based on two in-series birefringent optical fibers"

Osorio, J. H.*; Cordeiro, C. M. B.*

An optical fiber sensor based on the combination of two spliced birefringent optical fiber sections is proposed in this paper. The sensor is built up in a Solc-filter-like configuration and a simple theoretical model based on Jones matrices is employed to predict experimental results. By choosing the suitable birefringent optical fibers (e.g., photonic crystal fibers, birefringent microfibers, elliptical core fibers, PANDA fibers, etc.), the sensor described herein allows for probing of two physical parameters (e.g., refractive index and temperature, hydrostatic pressure and temperature) or sensing the same parameter in two disconnected environments. In order to demonstrate the sensor performance, the system response was evaluated in a temperature-sensing measurement.

Applied Optics 52[20], 4915-4921, 2013. DOI: 10.1364/AO.52.004915

[P224-2013] "Origin of magnetism in undoped TiO2 nanotubes"

Alivov, Y.; Grant, T.; Capan, C.; **Iwamoto, W.*; Pagliuso, P. G.***; Molloi, S.

Magnetic properties of undoped anatase, rutile, and amorphous titanium dioxide (TiO2) nanotubes grown by electrochemical anodization were studied by superconducting quantum interference device (SQUID) and electron spin resonance (ESR) methods in the temperature range 1.8-300 K.

All anatase, rutile, and amorphous TiO2 nanotubes were found to exhibit paramagnetic behaviors in the entire temperature range when tested with magnetic center concentrations of 6 x 10(17), 3 x 10(16), and 3 x 10(15) cm(-3), respectively. The diameter of the TiO2 nanotubes varied from 40-160 nm and has no significant effect on the magnetic properties observed. SQUID data showed strong nonlinear M-H relationships for anatase at low temperatures, and Arrot plot analysis suggested ferromagnetism in the sample with a Curie temperature T-C similar to 6 K. However, ESR studies showed no evidence for long-distance magnetic ordering. ESR studies revealed two magnetic centers with g(1) = 1 : 928 and g(2) = 2 : 028 that were common to all samples. The resonance peak at g1 = 1 : 922 was ascribed to Ti3+ cations centers resulting from oxygen vacancies, while the peak at g(2) = 2 : 028 was ascribed to surface absorbents. The amorphous sample ESR spectrum contained additional resonance peaks with corresponding g values at 2.228, 1.873, and 1.715 that possibly resulted from the disordered nature of these samples.

Nanotechnology 24[27], 275704, 2013. DOI: 10.1088/0957-4484/24/27/275704

[P225-2013] "Proton transport in water and DNA components: A Geant4 Monte Carlo simulation"

Champion, C.; Incerti, S.; Tran, H. N.; Karamitros, M.; Shin, J. I.; Lee, S. B.; Lekadir, H.; **Bernal, M.***; Francis, Z.; Ivanchenko, V.; Fojon, O. A.; Hanssen, J.; Rivarola, R. D.

Accurate modeling of DNA damages resulting from ionizing radiation remains a challenge of today's radiobiology research. An original set of physics processes has been recently developed for modeling the detailed transport of protons and neutral hydrogen atoms in liquid water and in DNA nucleobases using the Geant4-DNA extension of the open source Geant4 Monte Carlo simulation toolkit. The theoretical cross sections as well as the mean energy transfers during the different ionizing processes were taken from recent works based on classical as well as quantum mechanical predictions. Furthermore, in order to compare energy deposition patterns in liquid water and DNA material, we here propose a simplified cellular nucleus model made of spherical voxels, each containing randomly oriented nanometer-size cylindrical targets filled with either liquid water or DNA material (DNA nucleobases) both with a density of 1 g/cm(3). These cylindrical volumes have dimensions comparable to genetic material units of mammalian cells, namely, 25 nm (diameter) x 25 nm (height) for chromatin fiber segments, 10 nm (d) x 5 nm (h) for nucleosomes and 2 nm (d) x 2 nm (h) for DNA segments. Frequencies of energy deposition in the cylindrical targets are presented and discussed.

Nuclear Instruments & Methods In Physics Research Section B-Beam Interactions With Materials And Atoms 306, 165-168, 2013. DOI: 10.1016/j.nimb.2012.12.059

[P226-2013] "Purcell effect in sub-wavelength semiconductor lasers"

Gu, Q.; Slutsky, B.; **Vallini, F.*;** Smalley, J. S. T.; Nezhad, M. P.; **Frateschi, N. C.***; Fainman, Y.

We present a formal treatment of the modification of spontaneous emission rate by a cavity (Purcell effect) in sub-wavelength semiconductor lasers. To explicitly express the assumptions upon which our formalism builds, we summarize the results of non-relativistic quantum electrodynamics (QED) and the emitter-field-reservoir model in the quantum theory of damping. Within this model, the emitter-field interaction is modified to the extent that the field mode is modified by its environment. We show that the Purcell factor expressions frequently encountered in the literature are recovered only in the hypothetical condition when the gain medium is replaced by a transparent medium. Further, we argue that to accurately evaluate the Purcell effect, both the passive cavity boundary and the collective effect of all emitters must be included as part of the mode environment.

Optics Express 21[13], 15603-15617, 2013. DOI: 10.1364/OE.21.015603

[P227-2013] "Resonance running hologram velocity nonlinearity dependence upon light intensity in photorefractive crystals"

de Oliveira, I.; Carvalho, J. F.; **Frejlich, J.***

We report on the nonlinear relation between the resonance hologram velocity and the recording light irradiance in fringe-locked running hologram experiments carried out on a nominally undoped photorefractive Bi12TiO20 crystal using 532 nm wavelength laser light. Such nonlinearity is due to the dependence of the material diffusion length on the light irradiance. Experimental data show a good agreement with the theoretical equations thus supporting the mathematical model here reported and allowing to compute the quantum efficiency for photoelectron generation, the dependence of the diffusion length upon the recorded light irradiance, and the far from saturation diffusion length.

Applied Physics Letters 102[25], 251913, 2013. DOI: 10.1063/1.4812347

[P228-2013] "Search for a standard-model-like Higgs boson with a mass in the range 145 to 1000 GeV at the LHC"

Chatrchyan, S.; Khachatryan, V.; Sirunyan, A. M.; Tumasyan, A.; Adam, W.; **Chinellato, J.*; Tonelli Manganote, E. J.***; et al.
CMS Collaboration

A search for a standard-model-like Higgs boson in the H -> WW and H -> ZZ decay channels is reported, for Higgs boson masses in the range 145 < m(H) < 1000 GeV. The search is based upon proton-proton collision data samples corresponding to an integrated luminosity of up to 5.1 fb(-1) at root s = 7 TeV and up to 5.3 fb(-1) at root s = 8 TeV, recorded by the CMS experiment at the LHC. The combined upper limits at 95 % confidence level on products of the cross section and branching fractions exclude a standard-model-like Higgs boson in the range 145 < m(H) < 710 GeV, thus extending the mass region excluded by CMS from 127-600 GeV up to 710 GeV.

European Physical Journal C 73[6], 2469, 2013. DOI: 10.1140/epjc/s10052-013-2469-8

[P229-2013] "Search for narrow resonances using the dijet mass spectrum in pp collisions at root s=8 TeV"

Chatrchyan, S.; Khachatryan, V.; Sirunyan, A. M.; Tumasyan, A.; Adam, W.; Aguilo, E.; **Chinellato, J.*; Tonelli Manganote, E. J.*;** et al.
CMS Collaboration

Results are presented of a search for the production of new particles decaying to pairs of partons (quarks, antiquarks, or gluons), in the dijet mass spectrum in proton-proton collisions at root s = 8 TeV. The data sample corresponds to an integrated luminosity of 4.0 fb(-1), collected with the CMS detector at the LHC in 2012. No significant evidence for narrow resonance production is observed. Upper limits are set at the 95% confidence level on the production cross section of hypothetical new particles decaying to quark-quark, quark-gluon, or gluon-gluon final states. These limits are then translated into lower limits on the masses of new resonances in specific scenarios of physics beyond the standard model.

The limits reach up to 4.8 TeV, depending on the model, and extend previous exclusions from similar searches performed at lower collision energies. For the first time mass limits are set for the Randall-Sundrum graviton model in the dijet channel.

Physical Review D 87[11], 114015, 2013. DOI: 10.1103/PhysRevD.87.114015

[P230-2013] "Search for the standard model Higgs boson produced in association with a top-quark pair in pp collisions at the LHC"

Chatrchyan, S.; Khachatryan, V.; Sirunyan, A. M.; Tumasyan, A.; **Chinellato, J.*; Tonelli Manganote, E. J.***; et al.
CMS Collaboration

A search for the standard model Higgs boson produced in association with a top-quark pair is presented using data samples corresponding to an integrated luminosity of 5.0 fb(-1) (5.1 fb-1) collected in pp collisions at the center-of-mass energy of 7 TeV (8 TeV). Events are considered where the top-quark pair decays to either one lepton+jets (t (t) over bar -> l nu q (q) over bar 'b (b) over bar) or dileptons (t (t) over bar -> l(+)nu l-nu b (b) over bar), being an electron or a muon. The search is optimized for the decay mode H -> b (b) over bar. The largest background to the t (t) over barH signal is top-quark pair production with additional jets. Artificial neural networks are used to discriminate between signal and background events. Combining the results from the 7 TeV and 8 TeV samples, the observed (expected) limit on the cross section for Higgs boson production in association with top-quark pairs for a Higgs boson mass of 125 GeV is 5.8 (5.2) times the standard model expectation.

Journal Of High Energy Physics 5[145], 2013. DOI: 10.1007/JHEP05(2013)145

[P231-2013] "Second harmonic generation and enhancement in microfibers and loop resonators"

Gouveia, M. A.*; Lee, T.; Ismaeel, R.; Ding, M.; Broderick, N. G. R.; **Cordeiro, C. M. B.***; Brambilla, G.

We model and experimentally investigate second harmonic generation in silica microfibers and loop resonators, in which the second order nonlinearity arises from the glass-air surface dipole and bulk multipole contributions. In the loop resonator, the recirculation of the pump light on resonance is used to increase the conversion. The effect of the loop parameters, such as coupling and loss, is theoretically studied to determine their influence on the resonance enhancement. Experimentally, microfibers were fabricated with diameters around 0.7 mu m to generate the intermodally phase matched second harmonic with an efficiency up to 4.2 x 10(-8) when pumped with 5 ns 1.55 mu m pulses with a peak power of 90 W. After reconfiguring the microfiber into a 1 mm diameter loop, the efficiency was resonantly enhanced by 5.7 times.

Applied Physics Letters 102[20], 201120, 2013. DOI: 10.1063/1.4807767

[P232-2013] "Static and dynamic properties of Fibonacci multilayers"

Machado, L. D.*; Bezerra, C. G.; Correa, M. A.; Chesman, C.; Pearson, J. E.; Hoffmann, A.

We theoretically investigate static and dynamic properties of quasiperiodic magnetic multilayers. We considered identical ferromagnetic layers separated by non-magnetic spacers with two different thicknesses chosen based on the Fibonacci sequence. Using parameters for Fe/Cr, the minimum energy was determined and the equilibrium magnetization directions found were used to calculate magnetoresistance curves. Regarding dynamic behavior, ferromagnetic resonance (FMR) curves were calculated using an approximation known from the literature. Our numerical results illustrate the effects of quasiperiodicity on the static and dynamic properties of these structures.

Journal Of Applied Physics 113[17], 17C102, 2013. DOI: 10.1063/1.4794190

[P233-2013] "Structural and Magnetic Properties of Dilute Magnetic Oxide Based on Nanostructured Co-Doped Anatase TiO2 (Ti1-xCoxO2-delta)"

de Souza, T. E.; Mesquita, A.; de Zevallos, A. O.; **Beron, F.*; Pirota, K. R.***; Neves, P. P.; Doriguetto, A. C.; de Carvalho, H. B.

Nanostructured Co-doped anatase TiO2 (Ti1-xCoxO2-delta) samples were prepared and studied with particular emphasis on their compositional, structural, and magnetic properties. A detailed microstructural analysis was carried out to investigate the nature of the Co incorporation into the anatase TiO2 matrix. By combining different techniques, we confirmed the replacement of Ti4+ by Co2+ ions in the anatase TiO2 structure. Neither segregated secondary phases nor Co-rich nanocrystals were detected. Co doping was found to introduce oxygen vacancies into the system by means of a charge-compensation process. Superconducting quantum interference device magnetometry demonstrated paramagnetic Curie-Weiss behavior with antiferromagnetic interactions even in the presence of a high density of oxygen vacancies. The fitting of the M(H) curves in the limits of low and high temperatures enable the fractions of isolated and antiferromagnetically coupled Co ions to be extracted. We discuss the observed magnetic behavior of our samples considering the current main theories for the magnetic properties of dilute magnetic oxides.

Journal Of Physical Chemistry C 117[25], 13252-13260, 2013. DOI: 10.1021/jp4017129

[P234-2013] "Structural Investigation of the Surface of Bioglass 45S5 Enriched with Calcium Ions"

Lopes, J. H.; Mazali, I. O.; **Landers, R.***; Bertran, C. A.

In this article the changes on the surface of the 45S5 bioglass submitted to an enrichment with calcium ions were investigated. The method employed was the immersion of bioglass in calcium molten salt bath at 450 degrees C. Changes in composition were probed by different techniques of chemical analysis. The use of SEM-EDS allowed estimating the thickness modified, as being about 10m. X-ray photoelectron spectroscopy enabled to infer over the structural changes on the surface of 45S5 bioactive glass. The entry of calcium in the vitreous network promoted the phase separation of microdomains rich in silica and phosphate on the surface of the glass. The formation of immiscibility region was attributed a depolymerization of silica network and also, to a possible migration of phosphate species from the bulk. The results of this study indicate a great change in the surface properties of this biomaterial. In addition, the method proposed in this study proved to be very promising in the possibility of designing the surface of bioactive glasses, to modulate the desired properties, keeping the bulk unchanged.

Journal Of The American Ceramic Society 96[5], 1464-1469, 2013. DOI: 10.1111/jace.12305

[P235-2013] "Structural, optical and magnetic properties of Zn-1 (-) xCoxO prepared by the sol-gel route"

Srinet, G.; Varshney, P.; Kumar, R.; Sajal, V.; Kulriya, P. K.; **Knobel, M.*; Sharma, S. K.***

Effects of Co doping on the structural, optical and magnetic properties of ZnO samples prepared by the sol gel method are reported.

The X-ray diffraction, X-ray photoelectron spectroscopy and UV-visible spectroscopy confirmed the substitution of Co ions on Zn sites without changing the wurtzite structure. No segregated secondary phases or Co rich clusters were detected. Optical absorption spectra of the samples exhibit a blue shift in the absorption band edge with increasing dopant concentration. The photoluminescence measurements show a blue shift in UV emission peak with the increase in Co concentration and a slight shift in the green emission band at around 509 nm which gets suppressed for higher sintering temperature. The field dependence of magnetization observed at room temperature exhibits clear ferromagnetic behavior. Efforts have been made to fit the experimental M-H data using the magnetic polarons model (BMP) which involves localized carriers and magnetic cations. The calculated concentration of the BMPs is found to be below the typical percolation threshold in ZnO. Thus BMP model alone is not sufficient to explain the room temperature ferromagnetic behavior in ZnO. To know the exact magnetic ordering in the system, we also attempted to fit temperature dependent magnetization curves with the Curie Weiss Law which shows antiferromagnetic ordering in all samples.

Ceramics International 39[6], 6077-6085, 2013. DOI: 10.1016/j.ceramint.2013.01.025

[P236-2013] "Structurally tuned multiferroic state in BiFeO3-based compounds"

Gotardo, R. A. M.; Cotica, L. F.; Santos, I. A.; Olzon-Dyonisio, M.; Souza, S. D.; Garcia, D.; Eiras, J. A.; **Coelho, A. A.***

Structurally tuned multiferroic state is demonstrated for BiFeO3-based compounds. The electric and magnetic orders are strongly affected by the coexistence of R3c and Cm phases, i.e., by structural softness through monoclinicity, which leads the multiferroism to be driven by the same cation. The Cm phase enhances the ferroelectric and magnetic responses through Bi/Ba-O and Fe/Ti-O bonds by influencing structural distortions and ion valence. We also show the strong correlations between ferroic orders, structural arrangements, and tuning of the ion valence in the perovskite B site.

Applied Physics A-Materials Science & Processing 111[2], 563-567, 2013. DOI: 10.1007/s00339-012-7258-y

[P237-2013] "Studies of jet mass in dijet and W/Z plus jet events"

Chatrchyan, S.; Khachatryan, V.; Sirunyan, A. M.; Tumasyan, A.; **Chinellato, J.*; Tonelli Manganote, E. J.***; et al.
CMS Collaboration

Invariant mass spectra for jets reconstructed using the anti-k(T) and Cambridge-Aachen algorithms are studied for different jet "grooming" techniques in data corresponding to an integrated luminosity of 5 fb(-1), recorded with the CMS detector in proton-proton collisions at the LHC at a center-of-mass energy of 7 TeV. Leading-order QCD predictions for inclusive dijet and W/Z+jet production combined with parton-shower Monte Carlo models are found to agree overall with the data, and the agreement improves with the implementation of jet grooming methods used to distinguish merged jets of large transverse momentum from softer QCD gluon radiation.

Journal Of High Energy Physics 5, UNSP 090, 2013. DOI: 10.1007/JHEP05(2013)090

[P238-2013] "Surface restructuring of Pt films on Au stepped surfaces: effects on catalytic behavior"

Prieto, M. J.*; Tremiliosi, G.

In this paper, the reconstruction of Pt films deposited on stepped Au(hkl) surfaces belonging to the [n(111) x (110)] family of planes has been studied. Pt films were deposited using the galvanic displacement procedure of a pre-deposited Cu monolayer. We experimentally found that the Pt film deposition onto Au(hkl) surfaces is not fully epitaxial suggesting an atomic arrangement different from the underlying substrate. Additionally, we found that even though voltammetric profiles are not much different from those reported in the literature for Pt single crystals having the same crystallographic orientation, there is a reconstruction of the Pt layers on all Pt/Au(hkl) surfaces upon CO adsorption/oxidation as indicated by comparing the active areas of the Pt films before and after stripping. Additional FTIR in situ experiments on ethanol oxidation confirm that film reconstruction affects the reaction by product yield modification.

Physical Chemistry Chemical Physics 15[31], 13184-13189, 2013. DOI: 10.1039/c3cp51513c

[P239-2013] "Surface-Enhanced Resonance Raman Scattering (SERRS) Using Au Nanohole Arrays on Optical Fiber Tips"

Andrade, G. F. S.; **Hayashi, J. G.***; Rahman, M. M.; Salcedo, W. J.; **Cordeiro, C. M. B.***; Brolo, A. G.

Circular and bow tie-shaped Au nanoholes arrays were fabricated on gold films deposited on the tips of single-mode optical fibers. The nanostructures were milled using focused ion beam with a high quality control of their shapes and sizes. The optical fiber devices were used for surface-enhanced resonance Raman scattering (SERRS) measurements in both back- and forward-scattering geometries, yielding promising performance in both detection arrangements. The effect of the hole shape on the SERRS performance was explored with the bow tie nanostructures presenting a better SERRS performance than the circular holes arrays. The results present here are another step towards the development of optical fiber tips modified with plasmonic nanostructures for SERRS applications.

Plasmonics 8[2], 1113-1121, 2013. DOI: 10.1007/s11468-013-9518-x

[P240-2013] "Synthesis and Characterization of BaFe2As2 Single Crystals Grown by In-flux Technique"

Garitezi, T. M.*; Adriano, C.*; Rosa, P. F. S.*; Bittar, E. M.*; Bufaical, L.*; de Almeida, R. L.*; Granado, E.*; Grant, T.; Fisk, Z.; Avila, M. A.; Ribeiro, R. A.; Kuhns, P. L.; Reyes, A. P.; **Urbano, R. R.*; Pagliuso, P. G.***

We report a detailed characterization of BaFe2As2 single crystals grown by a metallic In-flux technique, an alternative to well-established growth routes using FeAs self- or Sn-flux. Electrical resistivity, magnetic susceptibility, nuclear magnetic resonance, and energy dispersive spectroscopy measurements showed no evidence of flux incorporation. More importantly, our results demonstrate that BaFe2As2 single crystals grown by In-flux have extremely high quality. To explore the efficiency of the In-flux growth method, we have also prepared nearly optimally doped superconducting samples of Ba(Fe1 -x M (x))(2)As-2 (M = Co, Cu, Ni, and Ru). Among other interesting features, this alternative chemical substitution method has led to enhancement of the maximum T (c) for most dopings.

Brazilian Journal Of Physics 43[4], 223-229, 2013. DOI: 10.1007/s13538-013-0144-z

[P241-2013] "System-size dependence of transverse momentum correlations at root s(NN)=62.4 and 200 GeV at the BNL Relativistic Heavy Ion Collider"

Adamczyk, L.; Adkins, J. K.; Agakishiev, G.; Aggarwal, M. M.; **Derradi de Souza, R.*; Takahashi, J.*; Vasconcelos, G. M. S.***, et al.

Autor(es) grupo: STAR Collaboration

We present a study of the average transverse momentum (p(t)) fluctuations and p(t) correlations for charged particles produced in Cu + Cu collisions at midrapidity for root s(NN) = 62.4 and 200 GeV. These results are compared with those published for Au + Au collisions at the same energies, to explore the system size dependence. In addition to the collision energy and system size dependence, the p(t) correlation results have been studied as functions of the collision centralities, the ranges in p(t), the pseudorapidity eta, and the azimuthal angle phi. The square root of the measured p(t) correlations when scaled by mean p(t) is found to be independent of both colliding beam energy and system size studied. Transport-based model calculations are found to have a better quantitative agreement with the measurements compared to models which incorporate only jetlike correlations.

Physical Review C 87[6], 064902, 2013. DOI: 10.1103/PhysRevC.87.064902

[P242-2013] "Temperature limits in laser cooling of free atoms with three-level cascade transitions"

Cruz, F. C.*; Sundheimer, M. L.; Magno, W. C.

We employ semiclassical theoretical analysis to study laser cooling of free atoms using three-level cascade transitions, where the upper transition is much weaker than the lower one. This represents an alternate cooling scheme, particularly useful for group II atoms. We find that temperatures below the Doppler limits associated with each of these transitions are expected. The lowest temperatures arise from a remarkable increase in damping and reduced diffusion compared to two-level cooling. They are reached at the two--photon resonance, where there is a crossing between the narrow and the partially dark dressed states, and can be estimated simply by the usual Doppler limit considering the decay rate of the optical coherence between these states.

Physical Review A 87[6], 063409, 2013. DOI: 10.1103/PhysRevA.87.063409

[P243-2013] "Third harmonic flow of charged particles in Au plus Au collisions at root s(NN)=200 GeV"

Adamczyk, L.; Adkins, J. K.; Agakishiev, G.; Aggarwal, M. M.; Ahammed, Z.; **Derradi de Souza, R.*; Takahashi, J.*; Vasconcelos, G. M. S.*,** et al.
STAR Collaboration

We report measurements of the third harmonic coefficient of the azimuthal anisotropy, upsilon(3), known as triangular flow. The analysis is for charged particles in Au + Au collisions at root s(NN) = 200 GeV, based on data from the STAR experiment at the BNL Relativistic Heavy Ion Collider. Two-particle correlations as a function of their pseudorapidity separation are fit with narrow and wide Gaussians. Measurements of triangular flow are extracted from the wide Gaussian, from two-particle cumulants with a pseudorapidity gap, and also from event plane analysis methods with a large pseudorapidity gap between the particles and the event plane. These results are reported as a function of transverse momentum and centrality. A large dependence on the pseudorapidity gap is found. Results are compared with other experiments and model calculations.

Physical Review C 88[1], 014904, 2013. DOI: 10.1103/PhysRevC.88.014904

[P244-2013] "X-ray photoelectron diffraction study of relaxation and rumpling of ferroelectric domains in BaTiO3(001)"

Pancotti, A.*; Wang, J. L.; Chen, P. X.; Tortech, L.; Teodorescu, C. M.; Frantzeskakis, E.; Barrett, N.

The surface of a ferroelectric BaTiO3(001) single crystal was studied using synchrotron radiation induced x-ray photoelectron diffraction (XPD), x-ray photoelectron spectroscopy (XPS), atomic force microscopy (AFM), and low-energy electron diffraction (LEED). AFM, XPS, and LEED show that the surface is BaO terminated with a (1 x 1) reconstruction. The Ba 4d, Ti 2p, and O 1s XPD results were compared with multiple scattering simulations for out-of- (P+, P) and in-plane (P-in) polarizations using a genetic algorithm to determine atomic rumpling and interlayer relaxation. Linear combinations of the XPD simulations of the surface structure of each polarization state allow determination of the domain ordering. The best agreement with experiment is found for 55% P+, 38% P-, and 7% P-in. The rumpling is smaller at the surface than in the bulk, suggesting that both domain ordering and surface structural changes contribute to screening of the polarization.

Physical Review B 87[18], 184116, 2013. DOI: 10.1103/PhysRevB.87.184116

Proceedings

[P245-2013] "Multimodal Nonlinear Optical Microscopy used to Discriminate Human Colon Cancer"

Adur, J.*; Pelegati, V. B.*; Bianchi, M.; **de Thomaz, A. A.*;** Baratti, M. O.; Carvalho, H. F.; Casco, V. H.; **Cesar, C. L.*;** Periasamy A. (Ed.); Konig K. (Ed.); So PTC (Ed.)

Colon cancer is one of the most diffused cancers in the Western World, ranking third worldwide in frequency of incidence after lung and breast cancers. Even if it is curable when detected and treated early, a more accurate premature diagnosis would be a suitable aim for both cancer prognostic and treatment. Combined multimodal nonlinear optical (NLO) microscopies, such as two-photon excitation fluorescence (TPEF), second-harmonic generation (SHG), third harmonic generation (THG), and fluorescence lifetime imaging microscopy (FLIM) can be used to detect morphological and metabolic changes associated with stroma and epithelial transformation in colon cancer disease. NLO microscopes provide complementary information about tissue microstructure, showing distinctive patterns between normal and malignant human colonic mucosa. Using a set of scoring methods significant differences both in the content, distribution and organization of stroma collagen fibrils, and lifetime components of NADH and FAD cofactors of human colon mucosa biopsies were found. Our results provide a framework for using NLO techniques as a clinical diagnostic tool for human colon cancer, and also suggest that the SHG and FLIM metrics could be applied to other intestinal disorders, which are characterized by abnormal cell proliferation and collagen assembly.

Multiphoton Microscopy In The Biomedical Sciences XIII. Proceedings of SPIE, v. 8588, UNSP 85881J, 2013. DOI: 10.1117/12.2001708

Patente

[Pa003-2013] "Processo de obtenção de sensores de pressão e fontes de elétrons à base de carbono e controlados por pressão, e material de carbono obtido para confecção dos dispositivos"

CHUN HWA PATRICK POA; Rodrigo Gribel Lacerda; SEMBUKUTTIARACHILAGE RAVI PRADIP SILVA; **FRANCISCO DAS CHAGAS MARQUES***

Número da Patente ou Registro: (Agência INOVA) PI0203947-8
Tipo da Patente: de Invenção
Mês/Ano de Conclusão:07/2013 - INPI/BBRASIL

Fonte: SIPEX – Sistema de Informação e Pesquisa e Extensão da Unicamp.

Disponível em: http:///wwww.uunicamp.br/ssipex/

Artigos Aceitos para Publicação

[A006-2013] "Dose point kernels in liquid water: An intra--comparison between GEANT4-DNA and a variety of Monte Carlo codes"

Champion, C., Incerti, S., Perrot, Y., Delorme, R., Bordage, M.C., Bardiès, M., Mascialino, B., Tran, H.N., Ivanchenko, V., **Bernal, M.***, Francis, Z., Groetz, J.-E., Fromm, M., Campos, L.

Modeling the radio-induced effects in biological medium still requires accurate physics models to describe the interactions induced by all the charged particles present in the irradiated medium in detail. These interactions include inelastic as well as elastic processes. To check the accuracy of the very low energy models recently implemented into the GEANT4 toolkit for modeling the electron slowing-down in liquid water, the simulation of electron dose point kernels remains the preferential test. In this context, we here report normalized radial dose profiles, for mono-energetic point sources, computed in liquid water by using the very low energy "GEANT4-DNA" physics processes available in the GEANT4 toolkit. In the present study, we report an extensive intra-comparison of profiles obtained by a large selection of existing and well-documented Monte-Carlo codes, namely, EGSnrc, PENELOPE, CPA100, FLUKA and MCNPX.

Applied Radiation and Isotopes, 2013. DOI: 10.1016/j.apradiso.2013.01.037

[A007-2013] "Photo induced dissociation of amino acids free from thermal degradation effects: A case study applied to DL-Valine"

Silva, A.M.d., Mocellin, A., Farrokhpour, H., Mundim, M.S.P., **Brito, A.N.***

We present a careful study of the thermal degradation effects in the mass spectrum of DL-Valine using a quadrupole mass spectrometer and a time of flight - mass spectrometer. This allows setting the temperature of 95 ± 10 °C as threshold for the sublimation of our solid sample. Based on the assignments for each ionic fragment detected, it is possible to separate the mass peaks in groups, explaining what are the principal bond breaks involved in the specific ionic yield, whose procedure can be extended to other amino acids.

Journal of Electron Spectroscopy and Related Phenomena, 2013. DOI: 10.1016/j.elspec.2013.02.004

*** Autores do Instituto de Física "Gleb Wataghin" - IFGW**

Defesa de Dissetações - Mestrado

[D012-13]"Desenvolvimento de nano catalisadores para a catálise heterogênea na obtenção de gás de síntese a partir de bio-óleos"
Aluno: Alexandre Rodrigues Filizola
Orientador: Prof. Dr. Carlos Alberto Luengo
Data: 27/06/2013

[D013-13]"Matrizes de massa e violação CP"
Aluno: Larissa Gaydutschenko
Orientador: Prof. Dr. Orlando L. Goulart Peres
Data: 27/06/2013

[D014-13]"Fenomenologia em Modelos com Dimensões extras"
Aluno: Pedro Simoni Pasquini
Orientador: Prof. Dr. Orlando L. Goulart Peres
Data: 28/06/2013

[D015-13]"Desenvolvimento de plataformas ópticas para sensoriamento de amostras biológicas"
Aluno: Jonas Henrique Osóri
Orientador: Prof. Dr. Cristiano Monteiro de Barros Cordeiro
Data: 10/07/2013

[D016-13]"Luminescência do Eu^{3+} em a-SiNx:H"
Aluno: Giácomo Bizinoto Ferreira Bosc
Orientador: Prof. Dr. Leandro Russovski Tessler
Data: 15/07/2013

[D017-13]"Molecular Simulation: Methods and Applications"
Aluno: Rodrigo Moura Freitas
Orientador: Prof. Dr. Maurice de Konin
Data: 29/07/2013

Defesa de Teses - Doutorado

[T007-13] "Physical Properties of FeAs-based intermetallic compounds"
Aluno: Priscila Ferrari Silveira Rosa
Orientador: Prof. Dr. Pascoal José Giglio Pagliuso
Data: 26/07/2013

[T008-13] "Nonclassicality abd entanglement"
Aluno: Frank Eduardo da Silva Steinhoff
Orientador: Prof. Dr. Marcos César de Oliveira
Data: 30/07/2013

[T009-13] "The dark universe: Observables nd degeneracies"
Aluno: Mariele Katherine Faria Motta
Orientador: Prof. Dr. Pedro Cunha de Holand
Data: 02/08/2013

[T010-13] "Propriedades estruturais e energéticas de defeitos extensos no gelo Ih"
Aluno: Domingos Lopes da Silva Júnior
Orientador: Prof. Dr. Maurice de Koning
Data: 16/08/2013

Fonte: Portal IFGW/PPós-graduação.
Disponível em: http://portal.ifi.unicamp.br/eventos#date=2013-05-01,mode=month

*** Acesse o portal Abstracta** <http://abstracta.ifi.unicamp.br> e faça seu **cadastro como Leitor** para receber por email as novidades de cada novo número publicado.

Abstracta

Instituto de Física
Diretor: Prof. Dr. Daniel Pereira
Diretor Associado: Prof. Dr. Newton Cesario Frateschi
Universidade Estadual de Campinas - UNICAMP
Cidade Universitária Zeferino Vaz
13083-859 - Campinas - SP - Brasil
e-mail: secdir@ifi.unicamp.br
Fone: 0XX 19 3521-5300

Publicação

Biblioteca do Instituto de Física Gleb Wataghin
http://portal.ifi.unicamp.br/biblioteca

Diretora Técnica: Sandra Maria Carlos Cartaxo
Coordenador da Comissão de Biblioteca: Prof. Dr. André Koch Torres de Assis

Elaboração
Maria Graciele Trevisan (Bibliotecária)
graciele@ifi.unicamp.br

Projeto Gráfico
ÍgneaDesign

Impressão: Gráfica Central - Unicamp